# Low-Cost Thermal Point Clouds of Indoor Environments

Aiara Brea[1], Francisco J. García-Corbeira[1], Elisavet Tsiranidou[1], Gustavo C. Peláez[1], Lucía Díaz-Vilariño[1], Joaquín Martínez[1]

[1] CINTECX, Universidade de Vigo, GeoTECH Group. 36310 Vigo, Spain
(aiara.brea, franciscojavier.garcia.corbeira, elisavet.tsiranidou, gupelaez, lucia, joaquin.martinez)@uvigo.gal

**Keywords:** Apple Smart Devices, iPhone Pro, iPad Pro, 3D Modelling, scan-to-BIM, Mobile Mapping.

**Abstract**

The integration of low-cost thermal sensors with Apple Smart Devices supports the generation of 3D point clouds that include temperature indicators. This generates a new perspective for the study of buildings, allowing for fast and reliable examination of physical building structures. To the best of our knowledge, this study is the first to demonstrate the use of affordable sensors for 3D thermal point cloud generation. The study involved capturing data from the LiDAR and thermal sensors, followed by an extrinsic calibration process to align the datasets. Subsequently, the point cloud was segmented based on different acquisition poses of the device and finally, the thermal data was projected onto the 3D model, integrating temperature information with spatial coordinates. Our results demonstrate the effectiveness of the approach for three-dimensional point cloud generation in indoor environments, highlighting significant thermal variations and enabling thermal mapping of building structures. Furthermore, our findings underscore the feasibility of employing low-cost sensors for generating detailed thermal models, opening possibilities for widespread adoption in various building analysis applications. This approach provides a comprehensive and cost-effective solution for building monitoring, democratizing access to advanced evaluation tools.

## 1. Introduction

The evolution of scanning technology has undergone significant transformation in recent decades, characterized by a notable reduction in costs and an expansion of devices options. In particular, the emergence of LiDAR-equipped smartphones has ushered in a new era of accessibility, versatility, and connectivity in scanning technology. These advancements have paved the way for innovative applications in 3D mapping and augmented reality, both indoors and outdoors.

While considerable research has been conducted on the mapping and augmented reality potential of LiDAR-equipped smartphones (Luetzenburg, Kroon, and Bjørk 2021; Spreafico et al. 2021), there remains a notable gap in the literature regarding their integration with other sensors to enhance non-destructive building surveys.

Although various studies have demonstrated the efficacy of Apple LiDAR in structure evaluation (Błaszczak-Bąk et al. 2023; Díaz-Vilariño et al. 2022; Teo and Yang 2023), there is a scarcity of research explicitly addressing how LiDAR integration with other sensors can enrich the data collected in these surveys. This research gap suggests an opportunity to further explore and develop the application of this combined technology in building analysis, providing valuable insights into structural integrity, energy efficiency, and environmental conditions.

Infrared thermography is a widely adopted non-invasive technique for diagnosing building pathologies and assessing their energy behaviour. It enables the detection of problems that include air infiltration, moisture, thermal bridges, and failures in insulation systems (Almeida, Ornelas, and Cordeiro 2020; Olbrycht 2020). Apart from its usefulness, traditional infrared devices have been limited to just two-dimensional thermal images with low resolution, thus limiting professionals in terms of obtaining a detailed, comprehensive view of the structures under inspection.

During the last few years, the transition of thermography from 2D to 3D has captured the interest of researchers, enabling an opportunity to deepen building assessment by allowing the creation of three-dimensional thermal models. These models give a richer, more detailed view of the thermal and structural conditions, promoting a fuller interpretation of the data collected (Angelosanti, Kulkarni, and Sabato 2022; Hou et al. 2022; Pérez-Andreu et al. 2023).

Diverse studies have explored the potential of 3D thermography by devising methods for the automatic mapping of thermal data onto 3D point clouds (Adán, López-Rey, and Ramón 2023; Borrmann et al. 2014; Lagüela et al. 2012). However, none of these studies addressed the need to investigate the integration of low-cost systems. By making 3D thermography more affordable and accessible, this research can democratize access to advanced building evaluation techniques, benefiting a wide range of stakeholders.

The extrinsic calibration between low-cost sensors is crucial to ensuring accuracy and consistency in integrating thermographic data into 3D models. While conventional systems may offer higher volume and quality data, low-cost devices can achieve comparable precision in their measurements (Dong, Sloan, and Chappuies 2024; Hakim et al. 2023). This disparity in data quantity and quality underscores the importance of precise calibration, as it helps correct potential discrepancies between data captured by different sensors.

In this regard, precise calibration is essential to achieving the correct alignment of data captured by different sensors, ensuring reliable and consistent results in building evaluation. Various methods of extrinsic calibration between LiDAR and thermal cameras have been presented in the literature (Dalirani et al. 2023; Dalirani and El-Sakka 2024; Zhang et al. 2018). Calibrations like these are based on modality correspondences for the calibration process. The research specifically relied on correspondence methods for feature matching between modalities to conduct calibration.

This paper presents a novel approach by advocating for the integration of Apple Smart Devices with low-cost thermal sensors in order to create 3D thermal point clouds. This approach takes advantage of the computing power of smart phones and their ubiquitous presence in modern times to democratize the access of leading-edge building monitoring capabilities.

The rest of the paper is organized as follows. Section 2 presents the proposed approach, while Section 3 shows the experiments and results obtained from applying the method to real case studies. Lastly, Section 4 is devoted to conclude this work.

## 2. Method

This research focuses on the fusion of LiDAR and thermal imaging technologies to create a thermal point cloud. By leveraging both LiDAR and thermal cameras, this study aims to harness their complementary functionalities, providing essential data for diverse applications such as building inspection, environmental monitoring, and infrastructure management.

The methodological approach in this study covers the following main steps: data capture and pre-processing, calibration and processing, and projection of thermal data onto the point clouds.

### 2.1 Data capture and pre-processing

Regarding data capture, the following sensors were used:

- LiDAR iPhone 12 Pro: The LiDAR system employed in this study is an integrated version into the iPhone 12 Pro, capitalizing on its ability to measure distances using the Direct Time-of-Flight (D-ToF) principle. This sensor includes an emitter that projects laser pulses and a receiver that records the time taken for the pulses to return after reflecting off objects. This enables the acquisition of precise information regarding the distance between the sensor and the surrounding objects, enabling the generation of a detailed three-dimensional representation of the environment.

- Thermal camera FLIR Lepton 3.1R: This camera boasts a resolution of 160 x 120 pixels and a wide field of view of 95º horizontally and 76º vertically. This camera can detect and quantify the thermal radiation emitted by objects, making it possible the visualization of temperature fluctuations in the surroundings. This is useful for applications such as hotspot detection in electrical systems, the identification of heat leakage from buildings, and temperature monitoring in industrial settings.

To achieve effective integration of these sensors, a 3D-printed mount was designed and created to securely align the iPhone with the thermal camera (
Figure **1**). This setup guarantees that both devices are properly positioned. By aligning the sensors accurately, this custom mount simplifies the subsequent extrinsic calibration process.

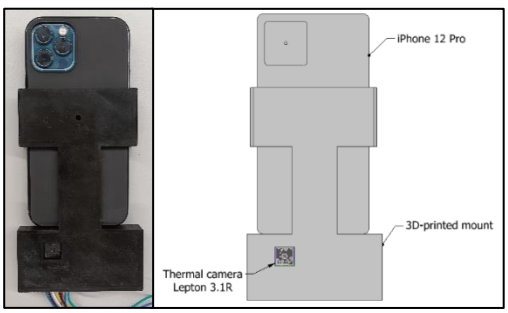


Figure 1: 3D-printed mount.

The data capture was conducted separately. We used 3D Scanner App to obtain the LiDAR point cloud. Within the app, the point cloud capture function is utilized to extract a whole folder of all the data information about the scan and a point cloud in PLY format. In this folder, there are diverse JSON format files from which the poses of each frame taken are extracted. Each pose is given by a transformation matrix $M$ as shown below:

$$\boldsymbol{M} = \begin{pmatrix} \boldsymbol{r_{11}} & \boldsymbol{r_{12}} & \boldsymbol{r_{13}} & \boldsymbol{p_x} \\ \boldsymbol{r_{21}} & \boldsymbol{r_{22}} & \boldsymbol{r_{23}} & \boldsymbol{p_y} \\ \boldsymbol{r_{31}} & \boldsymbol{r_{32}} & \boldsymbol{r_{33}} & \boldsymbol{p_z} \\ \boldsymbol{0} & \boldsymbol{0} & \boldsymbol{0} & \boldsymbol{1} \end{pmatrix} \quad (1)$$

The term pose refers to the relative position and orientation of an object in a three-dimensional space. In this context, the pose is used to describe the relative position and orientation of the data capture device (in this case, the iPhone with the LiDAR) with respect to the reference coordinate system of the point cloud. This reference coordinate system is defined by the LiDAR data, providing the spatial context for the captured frames.

Thermal images were captured by connecting the camera to a Raspberry Pi 3B+, where software was developed to capture the temperature matrix and the time at which frame was done (the acquisition time is 9 frame per second). This data is presented in an orderly manner inside a CSV file.

The infrared Lepton 3.1R features a 95º wide field of view (WFOV) lens, which can introduce barrel distortion. To correct this deformation, a rectification process is employed, ensuring a more accurate representation of the scene.

Once corrected, these images are presented in grayscale, which may hinder the interpretation of thermal data. To enhance visualization and facilitate the data analysis, a colour assignment process is performed for each normalized temperature value using the ‘jet’ colormap. This approach provides a more intuitive visual representation of the thermal distribution in the image, making it easier to identify areas of interest and interpret thermal data.

### 2.2 Calibration and processing

After data capture, the extrinsic calibration process plays a crucial role in our study. It aims to establish an alignment and spatial correlation between the data obtained from the thermal camera and the LiDAR sensor of the iPhone 12 Pro. This calibration procedure is essential for ensuring an accurate relationship between the datasets captured by these different sensors.

For the extrinsic calibration we used the feature matching method. This method involves the identification and use of common reference points in the data from both sensors. For this purpose, the corners of a wooden board were used as correspondence points.

To recognize them in the thermal image, four thermal resistors were place at each of the corners of a wooden board (
Figure **2**). These resistors were heated to reach a temperature of approximately 50ºC, creating significant contrast with the ambient temperature and being easily detectable in the thermal camera.

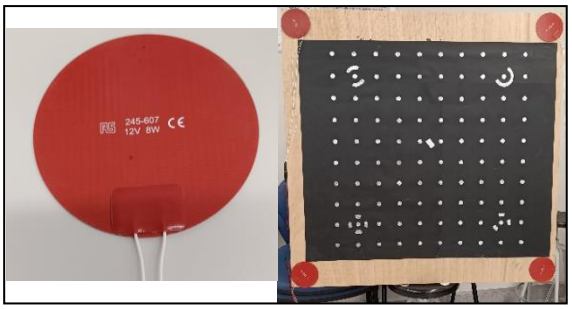

Figure 2: Thermal resistor and wooden board with resistors at each of its corners.

The thermal image processing for calibration is performed using the OpenCV library (Bradski 2000). Thermal points, appearing as blobs in the thermal image, were detected, and their contours were extracted. From these contours, the coordinates of the corners of the calibration board were calculated by creating a polygon between them.

Simultaneously, the point cloud obtained from LiDAR was processed to identify the corners of the same calibration board in three-dimensional space. This process involves several key steps. Using the Open3D library (Zhou, Park, and Koltun 2018), normal estimation in the point cloud is performed using a nearest neighbour-based search parameter. This helps to determine the orientation of surfaces in the point cloud.

Next, the point cloud is subdivided using the flat patch detection algorithm. This algorithm uses a statistically robust approach for flat patch detection. The process involves subdividing the point cloud into smaller blocks using an octree and then attempting to fit a plane to each block.

After identifying an initial set of planes, the plane of interest is selected based on an area range. Subsequently, the corners of the oriented bounding box are determined by identifying the extreme coordinates on the X and Y axes. This involves performing a Singular Value Decomposition (SVD) to find the normal of the plane, aiding in defining the orientation and spatial arrangement of the corners (Figure 3).

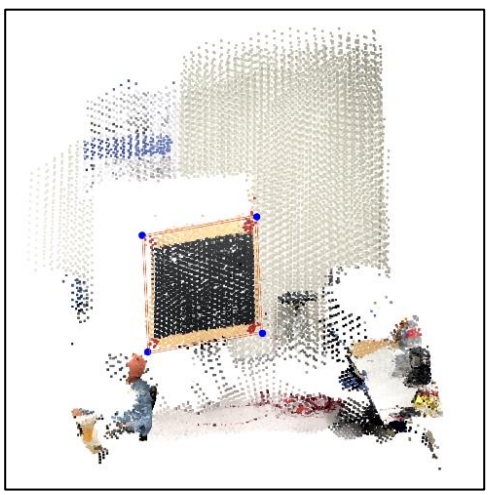

Figure 3: The corners of the bounding box, indicated in blue, are used for feature correspondence. Points are scaled for better visualization.

Before applying the Perspective-n-Point (PnP) method to calculate the transformation matrix that aligns the coordinate systems of the thermal camera and the point cloud, it's crucial to organize the obtained corners from the thermal image and the three-dimensional space. This ensures that both representations share the same order of corners for proper correspondence.

Once the corners are properly organized, the transformation matrix is calculated using the PnP method. The PnP method involves solving an equation that minimizes the reprojection error between the 3D and 2D point correspondences. The resulting transformation matrix $T$ can be represented as:

$$\boldsymbol{T} = [\boldsymbol{R}|\boldsymbol{t}] = \begin{pmatrix} \boldsymbol{r_{11}} & \boldsymbol{r_{12}} & \boldsymbol{r_{13}} & \boldsymbol{t_x} \\ \boldsymbol{r_{21}} & \boldsymbol{r_{22}} & \boldsymbol{r_{23}} & \boldsymbol{t_y} \\ \boldsymbol{r_{31}} & \boldsymbol{r_{32}} & \boldsymbol{r_{33}} & \boldsymbol{t_z} \\ \boldsymbol{0} & \boldsymbol{0} & \boldsymbol{0} & \boldsymbol{1} \end{pmatrix} \quad (2)$$

where $R$ is the rotation matrix and $t$ is the translation vector.

This transformation matrix can be used to convert a point $P_c$ from the coordinate system of the thermal camera to the point $P_{PC}$ in the point cloud coordinate system:

$$\boldsymbol{P_c} = \boldsymbol{R} \cdot \boldsymbol{P_{PC}} + \boldsymbol{t} \quad (3)$$

The transformation matrix $T$ can be computed using the PnP method in OpenCV (Bradski 2000). This process establishes a precise relationship between the data captured by different sensors, ensuring consistency and accuracy in integrating thermal data into the three-dimensional space of the point cloud.

To apply the parameters of the transformation to the point cloud after calibration, a method was implemented to segment the point cloud into sub-clouds based on various camera acquisition poses. Each pose provides a transformation matrix used to transform the global point cloud $PC_{PC}$ into the LiDAR device coordinate system:

$$\boldsymbol{PC_{LiDAR}} = \boldsymbol{R_p}^{\boldsymbol{T}}(\boldsymbol{PC_{PC}} - \boldsymbol{t_p}) \quad (4)$$

The $PC_{LiDAR}$ is segmented based on the Y coordinate of each point, keeping only those within a predefined range. Then, points in front of the camera are filtered using a dot product with a reference vector on the negative Z-axis. Finally, the filtered points are transformed back to the global coordinate system.

### 2.3 Projection of thermal data onto the point cloud

After segmentation, thermal image projection must be performed. For this, the segments must be translated and rotated to the initial calibration position. If $PC_2$ is the point cloud to be transformed to the reference system of the initial segment, the rotation matrices are $R_1$ and $R_2$ and translation vectors are $t_1$ and $t_2$, corresponding to the initial and final smartphone poses respectively, perform the necessary transformations:

$$\boldsymbol{PC_{trasf}} = \boldsymbol{R_1} \cdot \left(\boldsymbol{R_2}^{-1} \cdot (\boldsymbol{PC_2} - \boldsymbol{t_2})\right) + \boldsymbol{t_1} \quad (5)$$


https://doi.org/10.5194/isprs-archives-XLVIII-4-2024-99-2024  

These transformations ensure that the point cloud sub-clouds are correctly aligned with the initial system calibration, allowing for precise thermal image projection onto the scene captured by the LiDAR.

To project the thermal image onto the point cloud, the cv2.projectPoints function is first used to project the point cloud onto the image, obtaining the 2D coordinates of the projected points in the image.

Next, it iterates over the projected points and checks if they fall within the image boundaries. For points falling within the image, it extracts the corresponding colour and temperature from the image pixels. These values are stored in matrices for further processing.

After obtaining the colours and temperatures of the projected points, the colour values are converted from RGB to BGR and normalized to ensure they are in the range [0, 1]. An Open3D tensor is created containing information about the three-dimensional positions of the points, their temperatures, the projected colours, and the original colours. This tensor provides a structured representation of the data associated with the point cloud, facilitating its manipulation and analysis.

Each segment point cloud is relocated to its initial position and integrated into the resulting thermal point cloud. Additionally, the colours of the final point cloud are normalized to ensure that all segment point clouds use the same temperature range, homogenizing the temperature representation across the entire point cloud.

## 3. Results

Experimental tests were conducted to validate the effectiveness of the proposed methodology in integrating LiDAR and thermal data from low-cost sensors. In Figure 4, a representation of the thermal image with the corresponding polygon from the thermal blobs of the corners is observed. The corners of this polygon are used for extrinsic calibration.

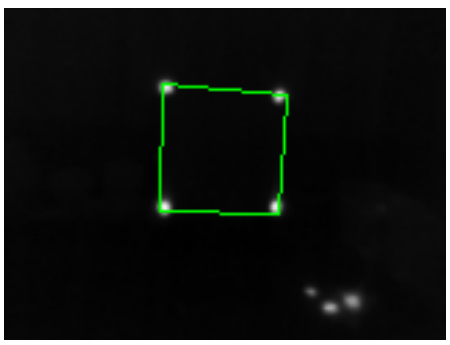

Figure 4: Thermal image with the corresponding blob detection polygon.

Figure 5 presents the same thermal image as Figure 4 but coloured with its respective normalized scale. This image provides a clear and detailed view of the temperature distribution in the captured environment, allowing for the identification of areas of significant thermal variations.

Figure 6 shows the complete point cloud generated only by rotating the support on the same axis. This visual representation provides insights into point density and distribution, showcasing the LiDAR’s ability to accurately map the three-dimensional environment.

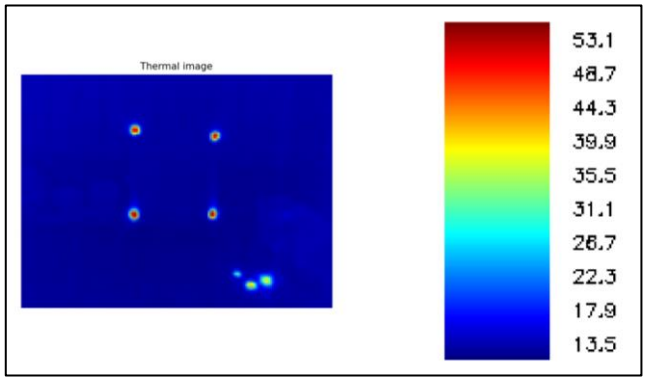


Figure 5: Thermal image coloured with its respective normalized temperature scale in ºC.

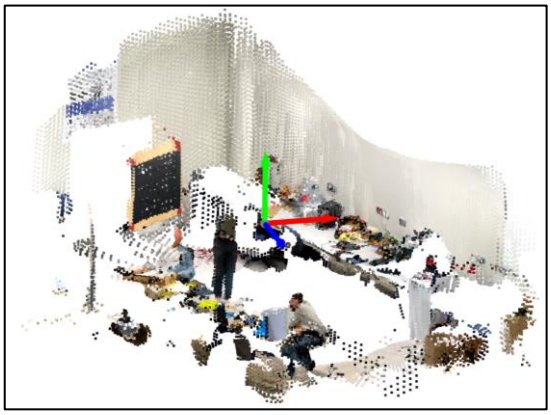

Figure 6: Complete point cloud from a capture on the same axis.

In Figure 8, the point cloud is segmented based on the pose of the smartphone. Six different segments have been created, allowing each thermal image to be projected in its corresponding location, as they are specified by the different LiDAR acquisition poses.

The transformation matrix provided in the Figure 7 represents the conversion between the coordinate systems of the first thermal image and the 3D point cloud. The first three columns correspond to the rotation and scaling components of the transformation, while the last column represents the translation component.

```
Transform matrix (T):
[[ 0.91917379  0.08780884 -0.383939    0.01299288]
 [ 0.12601323 -0.98915451  0.07545873  0.05478839]
 [-0.37314905 -0.11774108 -0.92026997  0.06960263]
 [ 0.          0.          0.          1.        ]]
```

Figure 7: Transformation matrix obtained from extrinsic calibration

Considering the known orientation of the image (with x to the right and y downwards), and the coordinate system of the point cloud (with x downwards, y to the right, and z axes following the right-hand rule), the rotation matrix appears to correctly align the axes of the two systems.


https://doi.org/10.5194/isprs-archives-XLVIII-4-2024-99-2024  

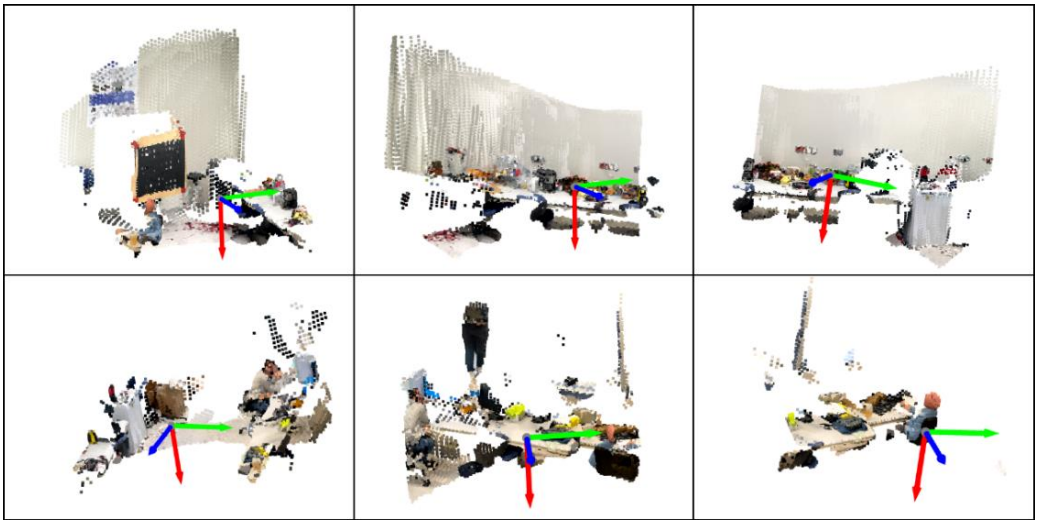

Figure 8: Point cloud segments.

Furthermore, the translation component of the matrix suggests a minimal displacement, which aligns with the physical setup where the LiDAR and thermal camera are closely mounted together.

In conclusion, the provided transformation matrix from the automatic extrinsic calibration accurately reflects the relationship between the coordinate systems of the thermal image and the point cloud, considering their respective orientations and physical setup.

In Figure 9 shows the thermal point cloud with projected Lepton images, evidencing the successful integration of thermal data into the three-dimensional point cloud. This combined visualization provides a complete and detailed representation of temperature distribution in the captured environment.

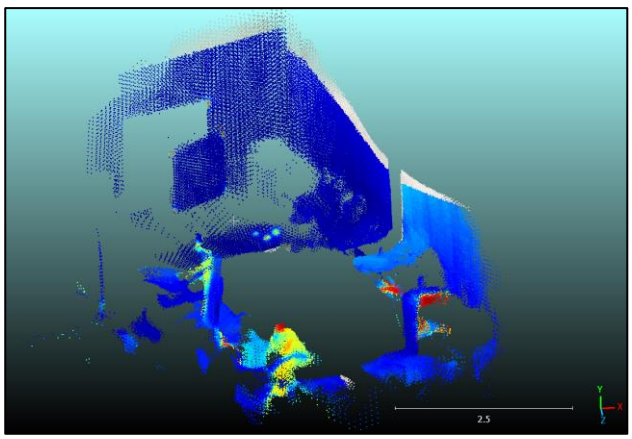

Figure 9: Thermal point cloud with projected RGB images.

Additionally, Figure 10 presents a histogram of temperatures from the point cloud, offering a graphical representation of the temperature distribution across the entire dataset. This visualization helps identify patterns and trends in the thermal distribution of the environment. It can be observed that most points are between 10°C and 25°C, and that points at 50°C are barely visible due to their insufficiency.

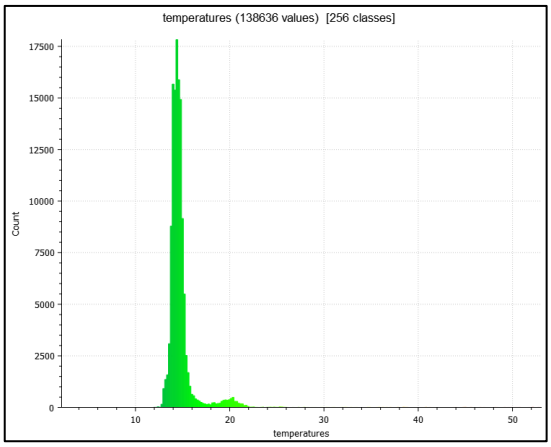


Figure 10: Temperature histogram of the point cloud.

Moreover, Figure 11 shows the point cloud with normalized RGB colours depending on the temperature, allowing a more intuitive visualization of temperature variations in the captured environment.

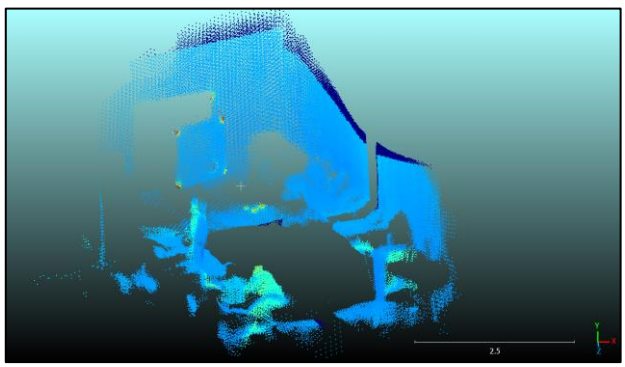

Figure 11: Point cloud with normalized RGB dependent on its temperature.

Figure 12 shows the point cloud with indicated temperatures and their corresponding scale in Cloud Compare. This detailed representation of the temperatures associated with each point in the point cloud facilitates a precise interpretation of the thermal data.

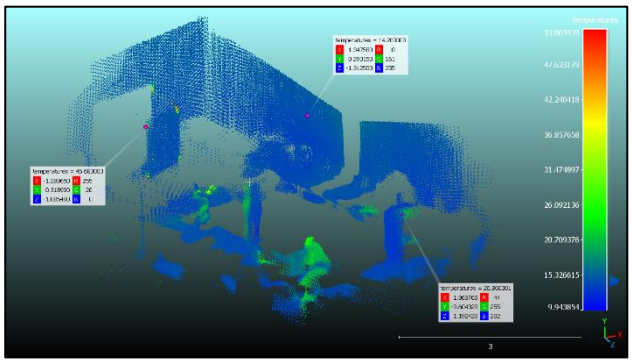

Figure 12: Point cloud with indicated temperatures and their scale in Cloud Compare.

Finally, Figure 13 and Figure 14 show the thermal point cloud captured by translating the device, as well as that same point cloud indicating its temperatures with a scale. These results complement the understanding of the thermal behaviour of the environment under different conditions and capture positions.

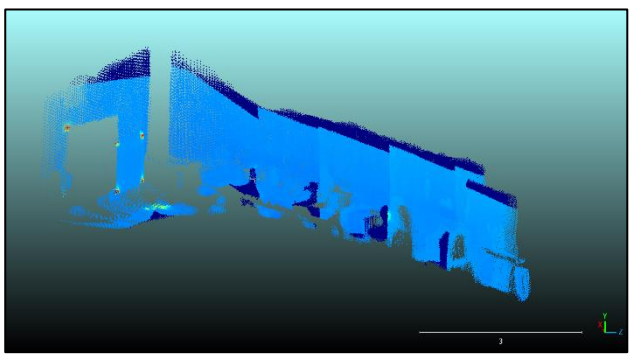

Figure 13: Thermal point cloud captured by translating the device.

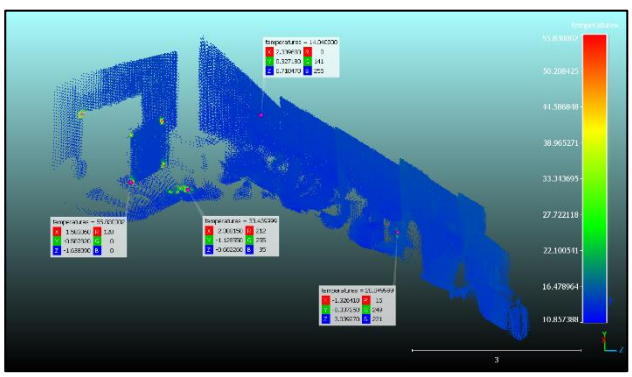

Figure 14: Thermal point cloud captured by translating the device indicating its temperatures with scale.

These findings represent significant advances in the integration of LiDAR and thermal camera data, with potential applications in a wide range of fields, including infrastructure inspections, environmental monitoring, and energy efficiency analysis in buildings.

## 4. Conclusions and future work

The research has successfully demonstrated the possibility of using LiDAR and low-cost thermal camera sensors for the generation of three-dimensional thermal point clouds. This approach democratizes access to advanced building monitoring technologies with the use of accessible devices like the iPhone 12 Pro and FLIR Lepton 3.1R thermal camera. The methodology developed in respect to data capture, processing, calibration, and integration of thermal data into the point cloud is efficient and provides accurate representation in three dimensions of the thermal distribution.

Furthermore, the provided transformation matrix from the automatic extrinsic calibration accurately reflects the relationship between the coordinate systems of the thermal image and the point cloud. The rotation matrix aligns the axes of the two systems appropriately, while the translation component indicates minimal displacement, in line with the physical arrangement of the LiDAR and thermal camera.

Results show projections of thermal images onto point clouds which demonstrate the potential of such integration to enhance infrastructure inspections, environment monitoring, and building energy efficiency analysis. The incorporation of the transformation matrix ensures consistency and accuracy in integrating thermal data into the three-dimensional space of the point cloud.

The potential of providing detailed three-dimensional thermal modelling opens new horizons in the comprehensive building evaluation and monitoring context, given structural integrity, energy efficiency, and environmental conditions.

Future work will focus on integrating these devices into a robotic platform for autonomous building thermal monitoring, in which additional thermal sensors will be employed, and efforts will be made to automate data capture.

## Acknowledgements

This work was partially supported by human resources grant RYC2020-029193-I funded by MCIN/AEI/10.13039/501100011033 and FSE ‘El FSE invierte en tu futuro’, by grant ED431F 2022/08 funded by Xunta de Galicia, Spain-GAIN, and by the projects PID2021-123475OA-I00, funded by MCIN/AEI/10.13039/501100011033/ FEDER/UE. We also acknowledge the funding by the European Union NextGenerationEU - Recovery and Resilience Mechanism (MRR/PRTR) through the grant TED2021-132000B-I00 of investment line I3. The statements made herein are solely the responsibility of the authors.

## References

Adán, Antonio, Alejandro López-Rey, and Amanda Ramón. 2023. ‘Robot for Thermal Monitoring of Buildings’. *Automation in Construction* 154 (October):105009. https://doi.org/10.1016/j.autcon.2023.105009.

Almeida, Ana Sofia Ferreira Coimbra e, Alexandre João Alves Ornelas, and António Rochette Cordeiro. 2020. ‘Termografia passiva no diagnóstico de patologias e desempenho térmico em fachadas de edifícios através de câmara térmica instalada em

drone. Abordagem preliminar em Coimbra (Portugal)’. *Cadernos de Geografia*, no. 42 (December), 27–41. https://doi.org/10.14195/0871-1623_42_2.

Angelosanti, Marco, Nitin Nagesh Kulkarni, and Alessandro Sabato. 2022. ‘Combination of Building Information Modeling and Infrared Point Cloud for Nondestructive Evaluation’. In *2022 IEEE International Workshop on Metrology for Living Environment (MetroLivEn)*, 269–73. https://doi.org/10.1109/MetroLivEnv54405.2022.9826970.

Błaszczak-Bąk, Wioleta, Czesław Suchocki, Tomasz Kozakiewicz, and Joanna Janicka. 2023. ‘Measurement Methodology for Surface Defects Inventory of Building Wall Using Smartphone with Light Detection and Ranging Sensor’. *Measurement* 219 (September):113286. https://doi.org/10.1016/j.measurement.2023.113286.

Borrmann, Dorit, Andreas Nüchter, Marija Đakulović, Ivan Maurović, Ivan Petrović, Dinko Osmanković, and Jasmin Velagić. 2014. ‘A Mobile Robot Based System for Fully Automated Thermal 3D Mapping’. *Advanced Engineering Informatics* 28 (4): 425–40. https://doi.org/10.1016/j.aei.2014.06.002.

Bradski, G. 2000. ‘The OpenCV Library’. *Dr. Dobb’s Journal of Software Tools*.

Dalirani, Farhad, and Mahmoud R. El-Sakka. 2024. ‘Extrinsic Calibration of Thermal Camera and 3D LiDAR Sensor via Human Matching in Both Modalities during Sensor Setup Movement’. *Sensors* 24 (2): 669. https://doi.org/10.3390/s24020669.

Dalirani, Farhad, Farzan Heidari, Taufiq Rahman, Daniel Singh Cheema, and Michael A. Bauer. 2023. ‘Automatic Extrinsic Calibration of Thermal Camera and LiDAR for Vehicle Sensor Setups’. In *2023 IEEE Intelligent Vehicles Symposium (IV)*, 1–7. https://doi.org/10.1109/IV55152.2023.10186694.

Díaz-Vilariño, L., H. Tran, E. Frías, J. Balado, and K. Khoshelham. 2022. ‘3D MAPPING OF INDOOR AND OUTDOOR ENVIRONMENTS USING APPLE SMART DEVICES’. *The International Archives of the Photogrammetry, Remote Sensing and Spatial Information Sciences* XLIII-B4-2022 (June):303–8. https://doi.org/10.5194/isprs-archives-XLIII-B4-2022-303-2022.

Dong, Younsuk, Guy Sloan, and Jack Chappuies. 2024. ‘Open-Source Time-Lapse Thermal Imaging Camera for Canopy Temperature Monitoring’. *Smart Agricultural Technology* 7 (March):100430. https://doi.org/10.1016/j.atech.2024.100430.

Hakim, N. N. A. Nik Azhan, R. Razali, M. S. Mohd Said, M. a. H. Muhamad, H. Abdul Rahim, and M. A. Mokhtar. 2023. ‘Accuracy Assessment on Detail Survey Plan Using iPhone 13 Pro Max LiDAR Sensor’. *International Journal of Geoinformatics* 19 (5): 79–86. https://doi.org/10.52939/ijg.v19i5.2665.

Hou, Yu, Meida Chen, Rebekka Volk, and Lucio Soibelman. 2022. ‘Investigation on Performance of RGB Point Cloud and Thermal Information Data Fusion for 3D Building Thermal Map Modeling Using Aerial Images under Different Experimental Conditions’. *Journal of Building Engineering* 45 (January):103380. https://doi.org/10.1016/j.jobe.2021.103380.

Lagüela, S., J. Armesto, P. Arias, and A. Zakhor. 2012. ‘AUTOMATIC PROCEDURE FOR THE REGISTRATION OF THERMOGRAPHIC IMAGES WITH POINT CLOUDS’. *The International Archives of the Photogrammetry, Remote Sensing and Spatial Information Sciences* XXXIX-B5 (July):211–16. https://doi.org/10.5194/isprsarchives-XXXIX-B5-211-2012.

Luetzenburg, Gregor, Aart Kroon, and Anders A. Bjørk. 2021. ‘Evaluation of the Apple iPhone 12 Pro LiDAR for an Application in Geosciences’. *Scientific Reports* 11 (1): 22221. https://doi.org/10.1038/s41598-021-01763-9.

Olbrycht, R. 2020. ‘Thermographic Analysis of Building Structures by Passive Transient Measurements’. In *Proceedings of the 2020 International Conference on Quantitative InfraRed Thermography*. QIRT Council. https://doi.org/10.21611/qirt.2020.039.

Pérez-Andreu, Víctor, Antonio Adán Oliver, Carolina Aparicio-Fernández, and José-Luis Vivancos Bono. 2023. ‘Thermal Characterization of Buildings with As-Is Thermal-Building Information Modelling’. *Buildings* 13 (4): 972. https://doi.org/10.3390/buildings13040972.

Spreafico, A., F. Chiabrando, L. Teppati Losè, and F. Giulio Tonolo. 2021. ‘THE IPAD PRO BUILT-IN LIDAR SENSOR: 3D RAPID MAPPING TESTS AND QUALITY ASSESSMENT’. *The International Archives of the Photogrammetry, Remote Sensing and Spatial Information Sciences* XLIII-B1-2021 (June):63–69. https://doi.org/10.5194/isprs-archives-XLIII-B1-2021-63-2021.

Teo, Tee-Ann, and Chen-Chia Yang. 2023. ‘Evaluating the Accuracy and Quality of an iPad Pro’s Built-in Lidar for 3D Indoor Mapping’. *Developments in the Built Environment* 14 (April):100169. https://doi.org/10.1016/j.dibe.2023.100169.

Zhang, Jun, Prarinya Siritanawan, Yufeng Yue, Chule Yang, Mingxing Wen, and Danwei Wang. 2018. ‘A Two-Step Method for Extrinsic Calibration between a Sparse 3D LiDAR and a Thermal Camera’. In *2018 15th International Conference on Control, Automation, Robotics and Vision (ICARCV)*, 1039–44. https://doi.org/10.1109/ICARCV.2018.8581170.

Zhou, Qian-Yi, Jaesik Park, and Vladlen Koltun. 2018. ‘Open3D: A Modern Library for 3D Data Processing’. *arXiv:1801.09847*.